Published by Institute of Physics Publishing for SISSA/ISAS

Received: *May 29, 2002*
Revised: *July 2, 2002*
Accepted: *July 3, 2002*

Astrophysical magnetic field reconstruction and spectroscopy with ultra high energy cosmic rays

Diego Harari

Departamento de Física, FCEyN, Universidad de Buenos Aires
Ciudad Universitaria - Pab. 1, 1428, Buenos Aires, Argentina
Email: harari@df.uba.ar

Silvia Mollerach and Esteban Roulet

CONICET and Centro Atómico Bariloche
Av. Bustillo km 9.5, 8400, S.C. de Bariloche, Argentina
Email: mollerac@cab.cnea.gov.ar, roulet@cab.cnea.gov.ar

Abstract: The next generation of ultra high energy cosmic ray experiments will probably detect several dozens of events clustered around the direction towards each of the most powerful extragalactic sources. We develop a method which could make possible to reconstruct, from the arrival directions and energies of the clustered events, the strength and coherence properties of the magnetic field along the line of sight towards the sources. The method exploits peculiar signatures arising from magnetic lensing effects, such as the strong flux magnification of multiple images around caustics. We also discuss how to obtain information about the cosmic ray composition, and apply this method to samples of simulated data.

Keywords: High Energy Cosmic Rays, Lensing, Electromagnetic Processes and Properties.

JHEP07(2002)006

Contents

1. **Introduction** 1

2. **Magnetic lensing** 2

3. **Magnetic field reconstruction** 4

4. **Conclusions** 10

1. Introduction

The origin and nature of ultra high energy cosmic rays (UHECRs), after several decades of study, is still puzzling [1, 2]. If they are charged particles, such as protons or heavier nuclei, their trajectories are affected by the magnetic fields along their path from the sources to the observer. For energies below $Z \times 10^{18}$ eV (Ze is the CR electric charge) they are confined by Galactic magnetic fields. For larger energies the galactic field is not strong enough to confine them, which combined with the lack of any significant excess from the galactic disk suggests that UHECRs are most probably of extragalactic origin. However, due to the effects of the magnetic fields present along their path, they do not point to their birth places, complicating the task of identifying their sources. The small angular scale clustering observed in the AGASA data [3] already hints to the existence of UHECR point sources [4, 5, 6], but the small present statistics does not allow to solve the source identification question. With the next generation of detectors, like AUGER [7] and EUSO [8], larger clusters are expected, having each several dozens of events. If this were the case, it would not only become possible to reconstruct the source positions, but also the data could be used to obtain information about the magnetic field along the CR path [9]–[12].

In this paper we discuss some strategies which can be adopted to reconstruct the main parameters of magnetic fields from a set of events originating from an extragalactic point source, and test them using simulated data. The knowledge of the magnetic field responsible for the deflections allows to better reconstruct the locations of the sources and, moreover, can also be helpful to do spectroscopy of CRs, making possible the measurement of their charges. The method we develop here profits from several specific features imprinted on the events by the magnetic fields, which not only deflect the trajectories but also lead to strong lensing phenomena, including the formation of multiple images and energy dependent magnifications or demagnifications of the CR fluxes [13, 14, 15].

JHEP07(2002)006

2. Magnetic lensing

UHECRs coming from extragalactic sources are influenced by the magnetic fields present along their path. These in principle include the magnetic fields around the source itself, that permeating the intergalactic space and the field in our galaxy. Observational determinations are available only for the last one, while upper bounds have been established on the intergalactic component from the absence of significant Faraday rotation of faraway polarised sources. The magnetic field in the Galaxy is known to have a regular and a turbulent component [16]. The regular field in the disk follows the spiral arms structure, with reversals taking place from arm to arm. The local value is $B_{\rm reg} \simeq 2\,\mu$G. The possible existence of an extended halo field (of few kpc scale height) is not settled down yet. The typical deflection in the direction of propagation of a CR particle of charge Ze and energy E produced by a regular magnetic field is

$$\delta \simeq 8.1^\circ \frac{40\,\mathrm{EeV}}{E/Z} \left| \int_0^L \frac{\mathrm{d}\mathbf{s}}{3\,\mathrm{kpc}} \times \frac{\mathbf{B}}{2\,\mu\mathrm{G}} \right| , \tag{2.1}$$

where $1\,\mathrm{EeV} = 10^{18}\,\mathrm{eV}$.

The turbulent galactic magnetic field component has a root mean square amplitude larger than the regular field, $B_{\rm rms} \simeq 1 - 3B_{\rm reg}$, and the largest turbulence scale is $L_{\rm max} \simeq$ 100 pc, while the minimum one is believed to be much smaller ($L_{\rm min} \ll L_{\rm max}$). It is often modeled as a gaussian random field with a Kolmogorov spectrum [17] (i.e. such that the energy density satisfies $\mathrm{d}E/\mathrm{d}k \propto k^{-5/3}$). The mean deflection of particles moving in the turbulent field vanishes, while the root mean square deflection is given by [15]

$$\delta_{\rm rms} \simeq 1.4^\circ \frac{40\,\mathrm{EeV}}{E/Z} \frac{B_{\rm rms}}{4\,\mu\mathrm{G}} \sqrt{\frac{L}{3\,\mathrm{kpc}}} \sqrt{\frac{L_c}{50\,\mathrm{pc}}} , \tag{2.2}$$

where L_c is the coherence length. For a narrow band ($L_{\rm min} \simeq L_{\rm max}$) spectrum, one has $L_c \simeq L_{\rm max}/2$, while for a broad band ($L_{\rm max} \gg L_{\rm min}$) Kolmogorov spectrum it is $L_c \simeq L_{\rm max}/5$.

We have written the random and regular field deflections in terms of the characteristic values of the Galactic fields, but these can be easily rescaled to describe the deflections if any particular model of the intergalactic magnetic field is adopted. We will hereafter focus for simplicity on the galactic component, and at the end will comment on the general case in which the intergalactic magnetic fields may also lead to non-negligible effects.

From eqs. (2.1) and (2.2) we see that the regular field generally produces the dominant effect on the deflection, which leads to a coherent displacement of the apparent position of the source that is inversely proportional to the energy. Compared to this, the random field produces rather small changes in the arrival direction of the CRs. However, as the charged particles propagate through the magnetic field, they are not only deflected, but their flux is also focused or defocused due to the differential deflections of neighboring paths [13, 14], with the effects being larger at smaller energies. As lower energies are considered, CR particles from one source can have more than one path leading to the detector, each traversing an uncorrelated magnetic field patch, and this leads to the appearance of multiple images of the source. This typically occurs when $\delta_{\rm rms} \simeq L_c/L$ [9, 15], what allows to define a critical energy E_c, around and below which the formation of multiple images is very likely, through[1]

$$\delta_{\rm rms} \equiv \frac{E_c}{E}\frac{L_c}{L}\,. \tag{2.3}$$

Its numerical value is given by[2]

$$E_c \simeq Z\, 60\,{\rm EeV}\,\frac{B_{\rm rms}}{4\,\mu{\rm G}}\left(\frac{L}{3\,{\rm kpc}}\right)^{3/2}\sqrt{\frac{50\,{\rm pc}}{L_c}}\,. \tag{2.4}$$

The new images appear in pairs, at an angular distance $\sim L_c/L$ from the position of the original source image and with a large magnification of their fluxes. The peak in the amplification when new images appear leads to small angular scale clustering and to an excess of events in an energy bin close to E_c [14, 15].

The overall picture can be summarized as follows: the magnetic fields present along the CR trajectories change the mapping between the observed arrival directions and the source ones. At the highest energies, the effects are small and hence the mapping is close to the identity. Going down in energy, deflections arise due to the turbulent and the regular magnetic field components. The turbulent component leads to small rms deflections, but it gives rise to a network of lines in the sky around which the fluxes of potential sources would be significantly magnified. This network corresponds to the directions where folds in the mapping (caustics) develop. The caustics appear at energies near (and below) $2\,E_c$, giving rise to multiple images of the sources lying close to those directions [15]. The regular field, which is responsible for larger deflections, leads to a global displacement of this network of caustics relative to the source directions. As a result of this drift caused by the regular field, a given CR source will experience successive magnifications and demagnifications of its flux at different energies caused by the motion of the caustic network across the sky. For decreasing energies, the continuous appearance of new images also leads to additional peaks in the spectrum, and strong lensing effects associated to the regular field component will also show-up.

Notice finally that the presence of large magnetic fields around the source galaxy could also lead to lensing effects. However, the multiple images will not be resolvable and the overall changes in arrival direction induced will be negligible as seen from Earth. The only observable effect will be a possible energy dependent modulation in the CR fluxes.

[1] The regular field can also lead to multiple images, with its characteristic scale of homogeneity (few kpc) playing the role of the coherence length.

[2] If the amplitude of the turbulent field were not constant, but had instead some modulation along the Galaxy, the factor $B_{\rm rms}\sqrt{L}$ in eq. (2.2) should be replaced by $|\int_0^L {\rm d}s\, B^2_{\rm rms}(s)|^{1/2}$, and $B_{\rm rms}L^{3/2}$ in eq. (2.4) should be replaced by $\left[3\int_0^L {\rm d}x\, x\int_0^x {\rm d}s\; B^2_{\rm rms}(s)\right]^{1/2}$.

3. Magnetic field reconstruction

The properties of the magnetic deflections and lensing effects can be used to determine the magnetic field parameters from the study of clustered UHECR events having their origin in isolated point-like sources. For this purpose one should start by defining the regions containing the excess events (which have to be larger than at least a few times the angular resolution of the detector but yet not too large to avoid excessive background events coming from other independent nearby sources). Different strategies must be considered, depending on the relative strength of the effects due to regular and random components, and in what follows we develop several ideas to perform this reconstruction.

Consider first the likely case in which the deflection caused by a regular component (either galactic or extragalactic) is larger than the rms deflection imprinted by the turbulent galactic field. In this case, the overall angular motion of the source images as a function of energy can be used to reconstruct the integral along the line of sight to the source of the perpendicular component of the regular magnetic field. In order to do this, one first finds the overall direction of motion of the images caused by the regular field by fitting a straight line ($\alpha_y = a + b\alpha_x$) to the event coordinates $\alpha_{x,y}$. The integral along the line of sight of the perpendicular component of the regular magnetic field will just be at a right angle with respect to this line, and its absolute value can be obtained choosing now the coordinates $\alpha_{||}$ (in the direction along the deflections produced by the regular field) and $\alpha_\perp$ (orthogonal to it), and plotting $\alpha_{||}$ vs. $1/E$ for the set of selected events. One should have, ignoring at this step the random field component, that

$$\alpha_{||_i} \simeq \alpha_0 + \frac{Z_i}{E_i} K_\perp \tag{3.1}$$

with

$$K_\perp \equiv \pm |e \int_0^L \mathrm{d}\mathbf{s} \times \mathbf{B}^{\mathrm{reg}}| \simeq \pm 1.3^\circ (40\,\mathrm{EeV}) \left| \int_0^L \frac{\mathrm{d}\mathbf{s}}{\mathrm{kpc}} \times \frac{\mathbf{B}^{\mathrm{reg}}}{\mu\mathrm{G}} \right| . \tag{3.2}$$

If the CRs have all identical electric charge Z, the events would fit nicely to just one straight line, $\alpha_{||} = \alpha_0 + c/E$. The slope c would give the value of $Z\,K_\perp$, which essentially provides the magnitude and direction of the regular magnetic field orthogonal to the l.o.s. multiplied by its relevant scale length, modulo the CR electric charge. The value of α_0 just gives the original location of the source ($\alpha_{||} = \alpha_0$, $\alpha_\perp = 0$). After the source location is estimated, it proves convenient to change variables to $\alpha_{||} \to \mathrm{sign}(K_\perp)\,(\alpha_{||} - \alpha_0)$, defined such that it tends to zero at large energies and increases as E decreases. In what follows we will use the name $\alpha_{||}$ just to refer to this shifted variable.

We illustrate this procedure using simulated data, obtained through a ray shooting technique, in which a large number of antiparticles were thrown isotropically from Earth, their trajectories numerically integrated across a distance L within a homogeneous magnetic field plus a turbulent component, and were finally recorded only if they pointed within a small cone (of aperture $\sim \delta_{\mathrm{rms}}/10$) from the direction to a fixed 'source'. The source was assumed to inject CRs with a differential energy spectrum $\mathrm{d}N/\mathrm{d}E \propto E^{-2.7}$. About 100 simulated events with energy above 40 EeV were selected, assuming the detector efficiency to be energy-independent. We display the 'theoretical' results from the simulation

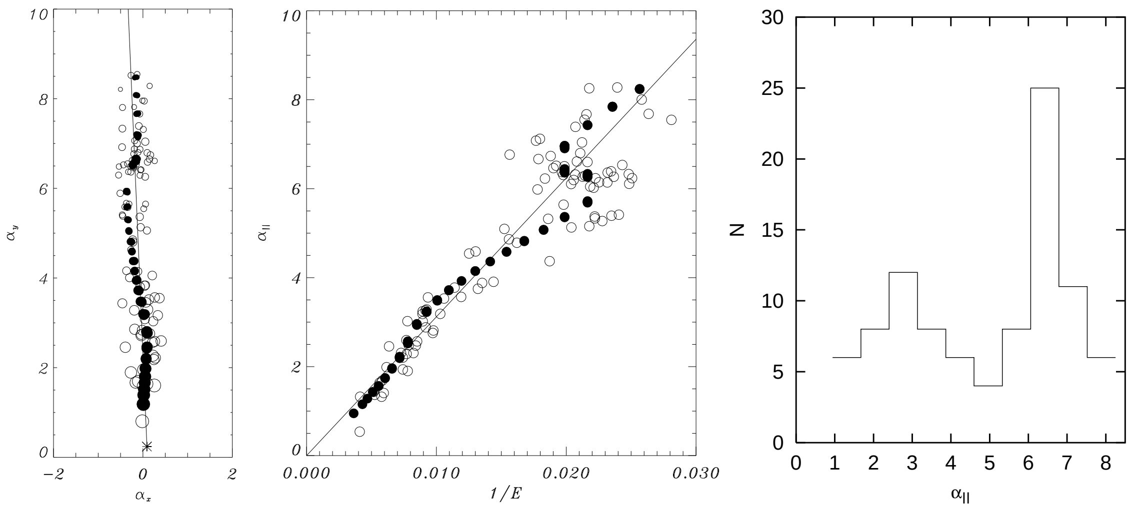

Figure 1: First Panel: Angular distribution of the simulated events for a regular field $B_{\rm reg} = 2\,\mu$G, a turbulent field with $B_{\rm rms} = 4\,\mu$G, $L_{\rm max} = L_{\rm min} = 100\,$pc and $L = 3\,$kpc. White circles have a gaussian noise with dispersion $0.2°$ added in each direction, as well as a 10% uncertainty in the energy, to simulate the detector sensitivity, while black circles have no noise added. The size of the circle grows with the energy of the event. The asterisk indicates the reconstructed position of the source, and the solid line the fit to the deflection due to the regular field. Second panel: $\alpha_\parallel$ vs. $1/E\,[{\rm EeV}^{-1}]$ and the linear fit to the data. Third panel: Number of events vs. $\alpha_\parallel$ divided in ten angular bins.

(with black dots) as well as more realistic ones (open circles) obtained by adding noise to the energy (corresponding to a detector energy resolution of 10%) and to the angles (corresponding to an angular resolution of $0.2°$ in each direction).

In the case illustrated in figure 1 the homogeneous magnetic field had strength $2\,\mu$G along the α_x direction, the turbulent component had $B_{\rm rms} = 4\,\mu$G with just one turbulence scale $L_{\rm max} = L_{\rm min} = 100\,$pc (and thus $L_c = 50\,$pc), and the distance traversed by the CRs (assumed to be protons) within these fields was $L = 3\,$kpc. The source actual position was in the direction $(\alpha_x = 0, \alpha_y = 0)$. The first panel displays the simulated data, with the straight line being the reconstructed overall direction of motion of the images and the star being the reconstructed source location. The second panel plots instead $\alpha_\parallel$ vs. $1/E$, while the third one will be discussed farther below.

In figure 2 we display the results for another simulation with the same parameters for the regular field and same root mean square amplitude of the turbulent field but with a Kolmogorov spectrum with $L_{\rm max} = 10 L_{\rm min} = 100\,$pc (corresponding to $L_c = 25\,$pc). The result for the best fit of the numerical reconstruction was for both cases $Z|\int_0^L {\rm d}\mathbf{s}\times\mathbf{B}| \approx 6.1\,\mu{\rm G\,kpc}$, in good agreement with the values used in the simulations.

In the case of a mixed composition, the fit of $\alpha_\parallel$ vs. $1/E$ to just one straight line should fail (excessive χ^2), since one expects to see the superposition of several straight lines, all with the same value of α_0 but different slopes, with ratios fixed by the ratio of the different electric charges Z_i involved.[3] In this case one can separate the events in groups,

[3]The value of α_0 in the case of mixed composition was just determined by eye, looking for the value of $\alpha_\parallel$ towards which the different lines converged.

JHEP07(2002)006

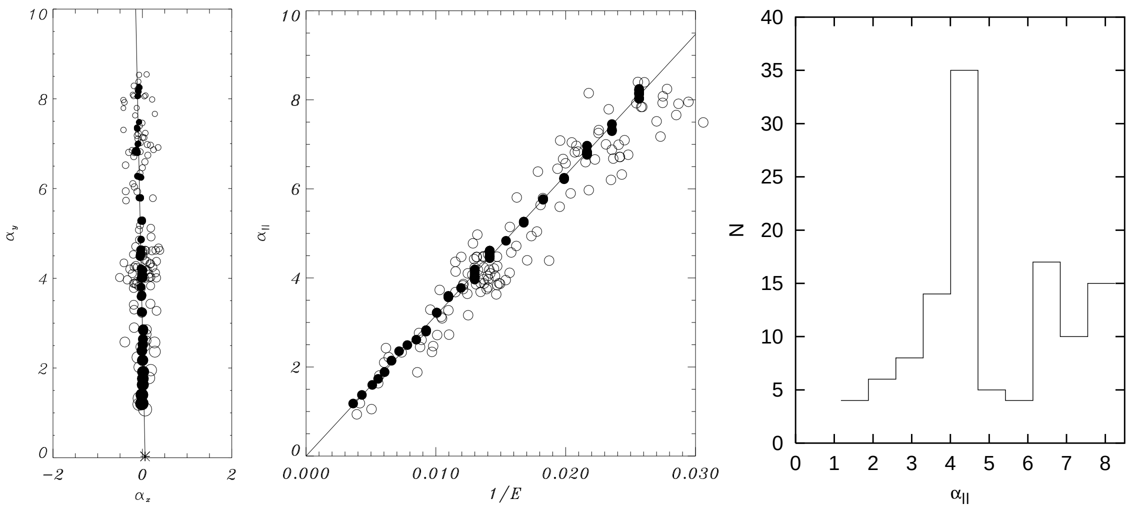

Figure 2: Same as figure 1 for a turbulent field with a Kolmogorov spectrum and $L_{\rm max} = 10L_{\rm min} = 100\,{\rm pc}$.

above and beyond limiting slopes, and then fit each group independently to an expression of the form given in eq. (3.1). This allows to obtain information on both $K_\perp$ and the ratio of charges Z_i involved, besides the relative amounts of different nuclei from the relative number of events on the different lines. Notice that the reconstructed fraction of different nuclei reflects the composition upon arrival to Earth, which may differ from the fraction injected by the source within the same energy range because the flux magnification due to magnetic lensing depends on the combination E/Z. Thus, the flux of different nuclei is magnified by a different factor at a given energy [14].

In figure 3 we exemplify this procedure for the same values of the fields and Kolmogorov spectrum with 60% of protons and 40% of Lithium ($Z = 3$). (The actual fraction of Lithium injected by the source was 50% in this case.) The two slopes in $\alpha_\|$ vs. $1/E$ are clearly separated and the reconstructed values are $Z_1|\int_0^L {\rm d}\mathbf{s}\times\mathbf{B}| \approx 5.9\,\mu{\rm G\,kpc}$, and $Z_2|\int_0^L {\rm d}\mathbf{s}\times\mathbf{B}| \approx 18.6\,\mu{\rm G\,kpc}$, implying that $Z_2/Z_1 \approx 3.1$.

In figure 4 we show the analogous results for 80% of protons and 20% of Helium, for which we obtain $Z_1|\int_0^L {\rm d}\mathbf{s}\times\mathbf{B}| \approx 6.2\,\mu{\rm G\,kpc}$, and $Z_2|\int_0^L {\rm d}\mathbf{s}\times\mathbf{B}| \approx 12.3\,\mu{\rm G\,kpc}$, implying that $Z_2/Z_1 \approx 2$. The reconstructed direction of the regular magnetic field was off by only a few degrees in all cases. Let us mention that we performed several other simulations with different realizations of the random field component, obtaining reconstructed values of similar quality.

Having determined the overall motion of the images due to the regular magnetic field component, we turn to analyze the effects of the turbulent field. At high energies the main effect is the formation of multiple images, with their associated peaks manifesting in the observed flux. The critical energy of this process, E_c (given by eq. (2.4)), can be determined from the location of the first lensing peak, which is expected to lie at energies somewhere between $2E_c$ and $E_c/2$. We then take bins in $\alpha_\|$ covering the range of angles

JHEP07(2002)006

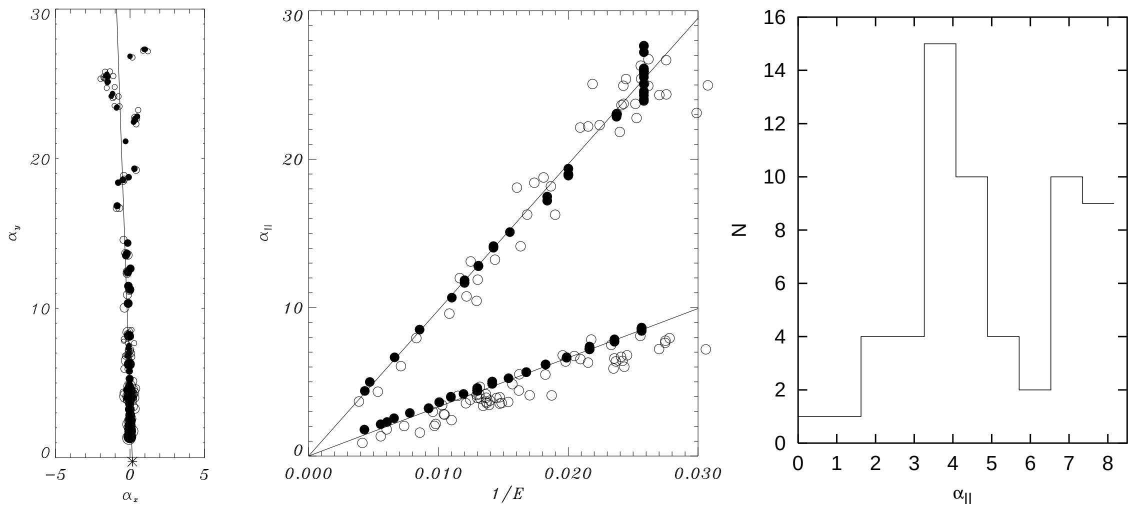

Figure 3: Same as figure 2 with mixed composition, 60% of protons and 40% of Lithium.

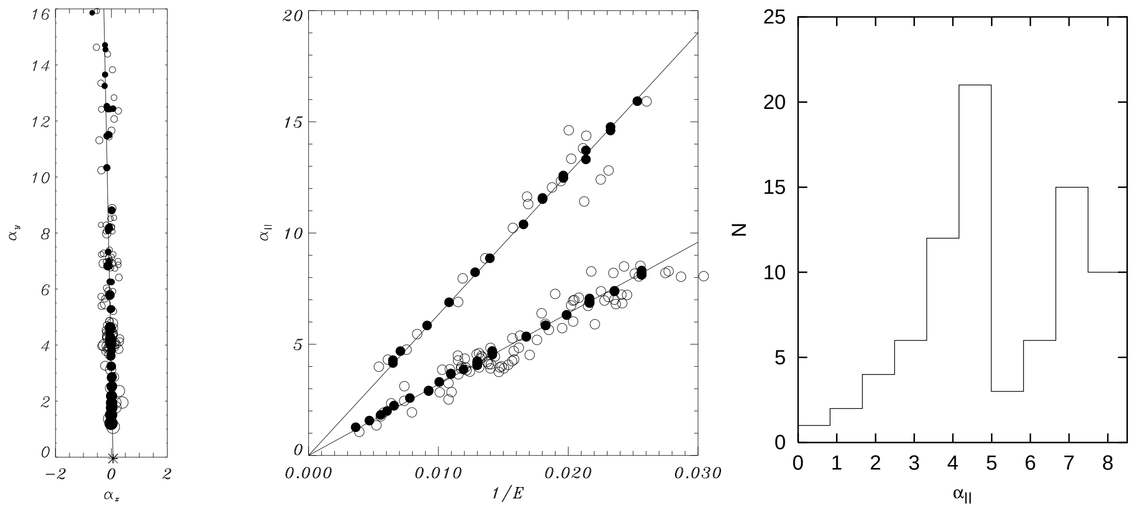

Figure 4: Same as figure 2 with mixed composition, 80% of protons and 20% of Helium.

where clustered events are observed above a certain energy threshold. The bins should be larger than the angular resolution of the detector and such that a sizeable number of events per bin result (taking e.g. ten angular bins if the number of clustered events is of the order of one hundred). Now one can plot the number of events in each bin vs. $\alpha_{\|}$. If there were only deflections but no flux (de)magnification due to lensing effects, the regular field would just lead to $\Delta N/\Delta\alpha_{\|} \propto \alpha_{\|}^{\beta}$, where β characterizes the slope of the CR energy spectrum, with $\mathrm{d}N/\mathrm{d}E \propto E^{-2-\beta}$.

The advantage of plotting ΔN in terms of $\alpha_{\|}$ (and not e.g. vs. E^{-1}) is that regardless of the CR composition the first lensing peak always appears at the same value of $\alpha_{\|}$.

Referring to this value as $\alpha_{\|}^{\text{peak}}$, one has then (up to an overall factor of two)

$$\frac{E_c}{Z} \simeq \frac{|K_\perp|}{\alpha_{\|}^{\text{peak}}} \tag{3.3}$$

The third panels of figures 1–4 illustrate the results of this method applied to the simulated data. In figure 1 the first lensing peak associated to multiple image formation appears at $\alpha_{\|}^{\text{peak}} \simeq 6.4°$ and corresponds to the sharp peak. It leads to a critical energy value $E_c/Z \approx 49\,\text{EeV}$, in good agreement with the parameters used in the simulation (which correspond to $E_c \approx 60\,\text{EeV}$). A shallower and more symmetric excess of events is also evident at smaller deflection angles, $\alpha_{\|}^{\text{peak}} \simeq 2.5°$, and it is due to a high magnification region crossing the source location at high energies (larger than $\approx 2E_c$, when folds were not yet formed).

In figure 2 the first peak appears at $\alpha_{\|}^{\text{peak}} \simeq 4.3°$, corresponding to $E_c/Z \approx 72\,\text{EeV}$ (while the simulation parameters lead to $E_c/Z \approx 85\,\text{EeV}$). For the mixed composition cases (figures 3 and 4) the corresponding values are $E_c/Z \approx 85\,\text{EeV}$ and $E_c/Z \approx 87\,\text{EeV}$ respectively.

The angular distribution of the events can also be used to estimate L_c/L (L here is the distance traversed along the turbulent component, which needs not be the same as that across the regular one). There are two independent ways to do this. One is based on the fact that at energies $\sim E_c$ the typical angular separation in the network of caustics of the turbulent magnetic field is $4L_c/L$ [15]. Since the effect of the regular field induced deflections is to move these caustics, relative to the source direction, the typical separation in $\alpha_{\|}$ between consecutive lensing peaks is also equal to $4L_c/L$. If at least two lensing peaks are observed in the data from one cluster, then L_c/L can be estimated. This is the case in the simulations presented above. In the case with just one wavelength depicted in figure 1 (which has $L_c = 50\,\text{pc}$), the separation between peaks is of order 4°, as it can be seen in the third panel, leading to $L_c/L \approx 0.017$. In the Kolmogorov spectrum cases (for which $L_c \simeq 25\,\text{pc}$) depicted in figures 2, 3 and 4, the separation among peaks is between 2° and 3°, leading to L_c/L values in the range 0.008–0.013. All these values are within 50% of the actual values used in the simulations.

Notice that it is likely to observe the first lensing peak rather close to $2E_c$, and to observe more than one lensing peak in the range of energies between $2E_c$ and $E_c/2$, if the deflection caused by the regular magnetic field component is strong enough. Indeed, the network of caustics is already well defined at energies around $2E_c$. Although only a small percentage of all potential source directions are sufficiently close to a caustic at energies around $2E_c$ to have their flux noticeably magnified, if the deflection caused by the regular magnetic field component is significant, a caustic will reach the source position at energies not far below $2E_c$. For instance, if the regular field deflection is at least 3 times larger than the rms deflection caused by the random field, then the source apparent position is displaced, as the energy decreases from $2E_c$ down to $E_c/2$, by more than $4L_c/L$. Since this is the typical separation between caustics, it is likely to produce more than one lensing peak in this energy range. Notice however that if the deflection by the regular field were too strong, the caustics may be crossed too fast, leading to a small integrated effect and thus a less noticeable peak.

JHEP07(2002)006

Alternatively, L_c/L can be determined from the fact that it is just the typical angular scale characterizing the separation between the images present in the first lensing peak. In this peak there are in principle one image corresponding to the principal image which is also present at higher energies, and two new images which are both in the same location of the sky and have appeared separated from the previous one by an angular scale of order L_c/L. Since this angular separation may be quite small, this approach can be used only when the angular uncertainty in the events is smaller than this scale. For the example shown in figure 1 this separation is about 1°, leading to an L_c/L estimate similar to the one obtained with the previous method. For the Kolmogorov spectrum cases, that leads to smaller L_c/L, we see from the first panel in figures 2, 3 and 4 that to apply this method in cases like these would require a quite precise angular resolution, probably better than the one achievable with AUGER ($\sim 0.3^\circ$), but possibly within the aim of some proposed detectors [18].

Once E_c/Z and L_c/L have been estimated, we can combine them to obtain an estimate of $B_{\rm rms}\,L$ using eq. (2.4). In our examples, the recovered values fall in the range $B_{\rm rms}\,L \simeq$ 10–13 μG kpc, in good agreement with the value 12 μG kpc used in the simulations.

If the deflection caused by the regular magnetic field is smaller than the rms deflection caused by the turbulent field at the same energy, the overall motion of the images does not provide reliable information about the regular magnetic field component, other than an upper bound on its integrated effect. However, it might still be possible to better reconstruct the source location by looking at the highest energy events, i.e. at energies above those at which the multiple images appear. Indeed, as long as the deflections are small ($\delta \ll L_c/L$), the random field component still produces a coherent deflection of the images proportional to $(E/Z)^{-1}$, and hence unless there is a significant mixture of different CR compositions there will be a clear signal allowing to reconstruct the source location. One could also extract information about the turbulent field through the spectral features imprinted by the lensing peaks, and by the angular clustering properties of the events. The critical energy E_c can be estimated as the highest energy at which a peak is observed in the spectrum. With sufficient angular resolution, L_c/L can be estimated from the angular separation between the images present in the first lensing peak, while information about the composition can be extracted from the observed energy ratios of the events clustered in the peaks [15].

These general features are illustrated in figure 5, which corresponds to a ray shooting simulation with a small orthogonal component of the regular magnetic field (leading to $\int B_\perp^{\rm reg} {\rm d}s = 0.3\,\mu$G kpc). The random component has $B_{\rm rms} = 4\,\mu$G (and spectrum with $L_{\rm min} = L_{\rm max} = 100$ pc) and $L = 3$ kpc. Events with energies larger than 40 EeV and injection spectrum $\propto E^{-2.7}$ are displayed. The left panel is for CR protons alone. The highest energy events move away from the source location (here the origin) with a deflection $\propto E^{-1}$, and at energies near 60 EeV two pairs of secondary images appear. They are displaced by $\sim 1.5^\circ$ from the principal image, hence leading to an estimated $L_c/L \simeq 0.026$, in good agreement with the input value 0.017. For the right panel, which has a mixed composition of protons and 40% Be at injection, other secondary images appear for $E >$ 40 EeV, dispersed over a region of $\sim 3^\circ$, and they contain exclusively the heavier Be nuclei,

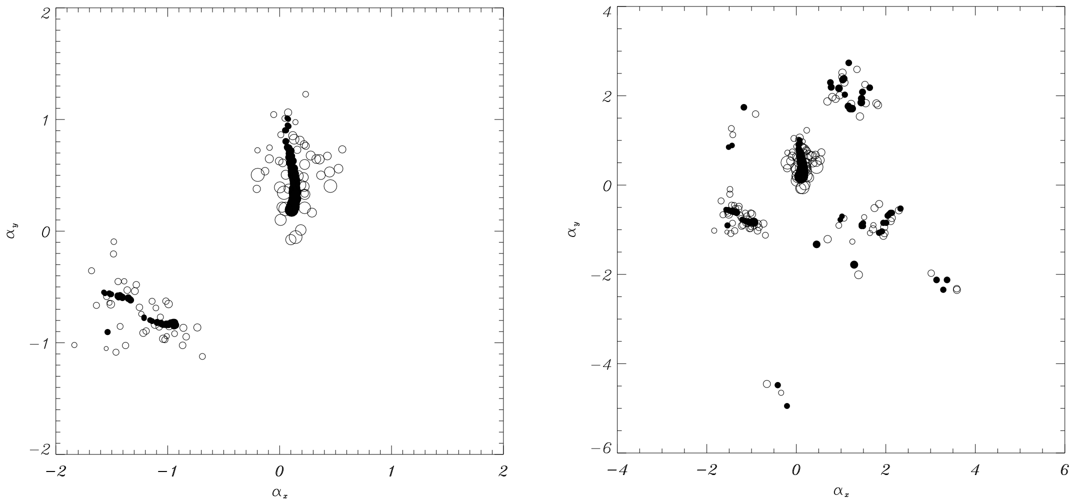

Figure 5: Simulated data in a regular field $B_{\rm reg} = 0.1\,\mu$G, and other parameters as in figure 1. The injected composition is 100% protons (left panel), and a mixture with 40% Beryllium (right panel).

since the protons in them have energies below 40 EeV. In general each of the secondary images has a narrow rigidity distribution due to the lensing origin of the peaks (and hence if two different elements were contributing to an image in the considered energy range, the events would split into groups with energy ratios given by the ratios of their charges).

4. Conclusions

One of the most exciting perspectives for the Auger Observatory currently under construction, as well as for other future experiments, is that they may inaugurate the era of UHECR astronomy. A hint that this may be the case is the small angular scale clustering observed by AGASA, which may be the first indication that a few UHECR sources are significantly more powerful than the otherwise apparently isotropic background.

UHECR astronomy is inevitably tied to the magnetic fields along the line of sight towards the most powerful sources, if the bulk of their emission is in the form of charged particles, such as protons or heavier nuclei. Conservative estimates of galactic and intergalactic magnetic fields indicate that the deflection of protons should be small at the highest energies, around and above 10^{20} eV, so that they should truly point to their birthplace. However, even protons with energies around 10^{20} eV may have their flux significantly (de)magnified by lensing effects, for instance by the turbulent component of the magnetic field in the Milky Way. A heavier component of UHECRs would undergo deflections larger than protons at comparable energies, and would be subject to similar flux (de)magnification effects at higher energies.

Consequently, the behaviour of the transition towards UHECR astronomy at the highest energies is a very rich source of information both on the source properties as well as on the characteristics of the intervening magnetic fields. This has been exploited, for instance in [11], as a tool for the reconstruction of intergalactic magnetic field parameters, particularly in the case of bursting sources of UHECRs [9], where the energy-dependent time delays provide additional handles to perform the task.

Here we developed a strategy to reconstruct the parameters of intervening magnetic fields that profits from the strong lensing effects that take place at energies of the order of E_c, given by eq. (2.4), around which it is likely to observe strongly magnified multiple images of single UHECR sources. We have shown that it is likely that a sort of 'magnetic spectroscopy' of UHECR sources may allow to measure the strength of the magnetic field along the line of sight, its coherence properties, and the relative amounts of nuclei with different electric charges among the observed CRs. Our analysis assumed the sources to be steady, what means here essentially that the typical time delays between different images are smaller than the timescales of emission of the sources.

The method works if the number, strength and location of sources, the UHECR composition, and the intervening magnetic field parameters are such that clusters with a large number (several dozens) of events can be identified, without excessive background from events with origin in nearby independent sources. The angular and energy resolution required is also dependent on the actual values of the parameters involved. We have shown, through illustrative examples based in simulated data, that the method is likely to be applicable for realistic values of the parameters of the galactic magnetic field. The overall angular motion of the events as a function of energy allows to reconstruct the integral along the line of sight of the perpendicular component of the regular magnetic field, modulo the CR electric charge. If this can be done for several sources, one may then even map the strength and extent of the magnetic field along different directions, and this could help to establish its overall distribution.[4] The reconstructed magnetic field also provides a handle to measure the relative number of CRs with different electric charges. A 'spectroscopic' analysis of the peaks in the number of events as a function of this overall motion (or as a function of energy when the effect of the regular component is not strong enough) provides a measure of the critical energy E_c/Z at which strong lensing phenomena occur. The enhanced angular clustering of the events at the energies where strong flux magnification takes place can also be used to estimate L_c/L, the ratio between the coherence length of the turbulent magnetic field component and the path length traversed by the CRs across it. E_c/Z and L_c/L provide a measure of $B_{\rm rms}L$, independent of the CR electric charge. The fact that the magnification peaks due to magnetic lensing occur at energies which are in direct proportion to the electric charge Z provides a second handle to grasp the CR composition. It induces a strong correlation of arrival directions at energy ratios fixed by the ratios of the CR electric charges.

Potentially, this method could also extract information about the different scales involved in the turbulence of the intervening magnetic field, if the experiments had sufficient energy and angular resolution (and, of course, statistics). If the spectrum is broad band, long and short wavelengths lead to amplification peaks at somewhat different values of

[4]Notice that the information reconstructed with UHECRs is complementary to that provided by Faraday rotation measurements, which are sensitive to the magnetic field component parallel to the line of sight.

JHEP07(2002)006

E/Z [15]. The density of lensing peaks could thus be used to obtain information on the magnetic field spectral properties. However, in realistic experiments the very narrow lensing peaks due to short wavelengths are likely to go unnoticed.

We illustrated how the reconstruction method works through simulated data built with magnetic field parameters relevant for the galactic case. The method may also provide information on extragalactic magnetic fields. For instance, lensing peaks at comparable energies would result due to propagation across a few times 10 Mpc in a turbulent magnetic field of rms strength 10^{-9} G, with coherence length of the order of 1 Mpc, since the associated critical energy is

$$E_c \simeq Z 2 \times 10^{19}\,\mathrm{EeV} \frac{B_{\mathrm{rms}}}{10^{-9}\,\mathrm{G}} \left(\frac{L}{10\,\mathrm{Mpc}}\right)^{3/2} \sqrt{\frac{\mathrm{Mpc}}{L_c}}\,. \tag{4.1}$$

Hence, if these magnetic fields have a large extent ($L \gg$ Mpc) and a significant strength ($\gg 10^{-9}$ G), their effects could produce noticeable signals at energies above 10^{20} eV even for protons, while for more modest fields, it would be the galactic magnetic fields the ones producing the dominant effects. Eventually, if an intergalactic or intracluster component were so strong that protons were already in the regime with a large number of images at ultra high energies, the source image would have an effective angular size of order δ_{rms} upon arrival to our Galaxy, which if large may average out the lensing effects within the galactic field, preventing its reconstruction with our method. Notice that the magnetic fields at the sources themselves may also have significant effects. These will not lead to identifiable multiple images from our observation point, but may produce an energy dependent beaming, which may have effects upon the observed spectrum similar to those we discussed. It may be potentially difficult to disentangle galactic from extragalactic contributions unless their characteristic critical energies are clearly separated. This may eventually depend on the source location, for instance if the turbulent component in the galactic disk overcomes the effects of the halo or extragalactic component for sources at relatively low galactic latitude. Different properties of the lensing peaks (characteristic energy, inter-peak separation) and of the multiple images (absence or presence, characteristic separation) may hopefully be indicative of galactic vs. extragalactic and regular vs. turbulent components.

Acknowledgments

Work partially supported by ANPCYT, CONICET, and Fundación Antorchas, Argentina.

References

[1] A.A. Watson, *Ultra-high-energy cosmic rays: the experimental situation*, *Phys. Rept.* **333** (2000) 309.

[2] A.V. Olinto, *Ultra high energy cosmic rays: the theoretical challenge*, *Phys. Rept.* **333** (2000) 329 [astro-ph/0002006].

[3] N. Hayashida et al., *Updated agasa event list above* 4×10^{19} *eV*, *Astrophys. J.* **522** (1999) 225 [astro-ph/0008102].

JHEP07(2002)006

[4] P.G. Tinyakov and I.I. Tkachev, *Correlation function of ultra-high energy cosmic rays favors point sources*, *Sov. Phys. JETP Lett.* **74** (2001) 1 [astro-ph/0102101].

[5] M. Takeda et al., *Clusters of cosmic rays above* 10^{19} *eV observed by AGASA*, in *Proc. ICRC* Hamburg, Germany 2001, p. 341;
M. Teshima, talk at TAUP 2001, Gran Sasso, Italy 2001, in press.

[6] C. Isola and G. Sigl, *Large scale magnetic fields and the number of cosmic ray sources above* 10^{19} *eV*, astro-ph/0203273.

[7] http://www.auger.org/

[8] http://euso-mission.org/

[9] E. Waxman and J. Miralda-Escude, *Images of bursting sources of high-energy cosmic rays: effects of magnetic fields*, *Astrophys. J.* **472** (1996) L89 [astro-ph/9607059].

[10] M. Lemoine, G. Sigl, A.V. Olinto and D.N. Schramm, *Ultra-high-energy cosmic-ray sources and large-scale magnetic fields*, *Astrophys. J.* **486** (1997) L115 [astro-ph/9704203].

[11] G. Sigl and M. Lemoine, *Reconstruction of source and cosmic magnetic field characteristics from clusters of ultra-high energy cosmic rays*, *Astropart. Phys.* **9** (1998) 65 [astro-ph/9711060].

[12] J. Alvarez-Muñiz, R. Engel and T. Stanev, *UHECR propagation in the galaxy: clustering versus isotropy* astro-ph/0112227.

[13] D. Harari, S. Mollerach and E. Roulet, *The toes of the ultra high energy cosmic ray spectrum*, *J. High Energy Phys.* **08** (1999) 022 [astro-ph/9906309].

[14] D. Harari, S. Mollerach and E. Roulet, *Signatures of galactic magnetic lensing upon ultra high energy cosmic rays*, *J. High Energy Phys.* **02** (2000) 035 [astro-ph/0001084].

[15] D. Harari, S. Mollerach, E. Roulet and F. Sánchez, *Lensing of ultra-high energy cosmic rays in turbulent magnetic fields*, *J. High Energy Phys.* **03** (2002) 045 [astro-ph/0202362].

[16] J. L. Han, *Magnetic fields in our galaxy: how much do we know?*, *Astrophys. Space Sc.* **278** (2001) 181 [astro-ph/0010537].

[17] J.W. Armstrong, J.M. Cordes and B.J. Rickett, *Density power spectrum in the local interstellar medium*, *Nature* **291** (1981) 561.

[18] M. Sasaki, A. Kusaka and Y. Asaoka, *Design of UHECR telescope with 1 arcmin resolution and 50 degree field of view*, astro-ph/0203348.

JHEP07(2002)006